Radiat Environ Biophys (2014) 53:273–282
DOI 10.1007/s00411-014-0525-x

ORIGINAL PAPER

Automated analysis of the cytokinesis-block micronucleus assay for radiation biodosimetry using imaging flow cytometry

M. A. Rodrigues · L. A. Beaton-Green · B. C. Kutzner · R. C. Wilkins

Received: 22 November 2013 / Accepted: 14 February 2014 / Published online: 7 March 2014

Abstract The cytokinesis-block micronucleus (CBMN) assay is employed in biological dosimetry to determine the dose of radiation to an exposed individual from the frequency of micronuclei (MN) in binucleated lymphocyte cells. The method has been partially automated for the use in mass casualty events, but it would be advantageous to further automate the method for increased throughput. Recently, automated image analysis has been successfully applied to the traditional, slide-scoring-based method of the CBMN assay. However, with the development of new technologies such as the imaging flow cytometer, it is now possible to adapt this microscope-based assay to an automated imaging flow cytometry method. The ImageStream^X is an imaging flow cytometer that has adequate sensitivity to quantify radiation doses larger than 1 Gy while adding the increased throughput of traditional flow cytometry. The protocol and analysis presented in this work adapts the CBMN assay for the use on the ImageStream^X. Ex vivo-irradiated whole blood samples cultured for CBMN were analyzed on the ImageStream^X, and preliminary results indicate that binucleated cells and MN can be identified, imaged and enumerated automatically by imaging flow cytometry. Details of the method development, gating strategy and the dose response curve generated are presented and indicate that adaptation of the CBMN assay for the use with imaging flow cytometry has potential for high-throughput analysis following a mass casualty radiological event.

Keywords Cytokinesis-block micronucleus (CBMN) assay · Automated MN analysis · Imaging flow cytometry · Biodosimetry · Population triage

M. A. Rodrigues · L. A. Beaton-Green · B. C. Kutzner · R. C. Wilkins (✉)
Consumer and Clinical Radiation Protection Bureau, Health Canada, 775 Brookfield Rd., Ottawa, ON K1A 1C1, Canada
e-mail: ruth.wilkins@hc-sc.gc.ca

M. A. Rodrigues
Department of Physics, Carleton University, Ottawa, ON K1S 5B6, Canada

Introduction

Radiation accidents or events involving large numbers of casualties can result from many different scenarios including nuclear power plant incidents such as Chernobyl and Fukushima, accidental overexposures involving medical or industrial devices, and terrorist attacks where radiological material is deployed. Radiation dose assessment is used to triage casualties of these events to determine proper medical treatment. Following a radiation accident, physical dosimetry through the use of dosimeters worn by exposed personnel can provide an indication of the dose. However, if the incident is more complex, such as the terrorist use of a dirty bomb, the number of people exposed can be substantial and physical dose estimations are not always possible to obtain. In these situations, biological dosimetry through scoring of chromosomal damage may be used to determine the dose received. In situations where dosimetry must be performed on large numbers of casualties, obtaining dose estimations relatively quickly is critical to determine the proper treatment course. Medical intervention is typically only required for patients receiving a dose of 1 Gy or higher; thus, cytogenetic assays that can rapidly and reliably identify this dose threshold are ideal (Lloyd et al. 2000).

Both the dicentric chromosome assay (DCA) (IAEA 2011; Lloyd et al. 2000) and the cytokinesis-block

micronucleus (CBMN) assay (McNamee et al. 2009; Vral et al. 2011) are proven dosimetric techniques that are robust and sensitive enough to provide accurate biological dose estimates. The DCA and the CBMN assay exploit the direct correlation between the number of dicentric chromosomes and micronuclei (MN), respectively, to dose. Historically, both methods are performed by manual slide scoring and are thus labor-intensive, time-consuming and subject to variability of interpretation between scorers. The DCA and the CBMN assay give accurate dose estimations but are not able to be performed quickly enough to be useful following a mass casualty radiation event in which the dose to hundreds or thousands of casualties may need to be determined. In this case, automated analysis of both the DCA and CBMN assay is desirable.

Methods of automating the DCA have been developed recently using both slide counting and imaging cytometry. Vaurijoux et al. (2009) showed that automated dicentric scoring using DCScore software (MetaSystems, Baden-Württemberg, Germany) proved to be more accurate than manual scoring for the purposes of rapid analysis of a large population. In addition, 1,000 metaphases were scored automatically in 1 h, where only 50 metaphases could be scored manually in the same time period. They also showed that a similar automated method could be used to analyze several thousand metaphases and can accurately quantify non-homogeneous partial-body exposures, typically seen in radiation accidents (Vaurijoux et al. 2012). Most recently, Beaton et al. (2013) investigated the potential of automating the DCA using imaging flow cytometry. Results of this work indicated that individual chromosomes could be identified, mono- and dicentric chromosomes could be differentiated, and a preliminary dose response curve was generated.

With respect to the automation of the CBMN assay, the framework for development began in the early 1990s. Castelain et al. (1993) generated an algorithm based on a sequence of grayscale and binary operators to score MN on Giemsa- and Feulgen-Congo Red-stained slides. Verhaegen et al. (1994) developed a similar algorithm using binary images developed from Romanowsky–Giemsa-stained slides, along with a combination of low- and high-magnification images to automatically detect MN. In recent years, a number of new methods that focus on fully automating the CBMN assay have been developed and applied to various fields such as biomonitoring (Rossnerova et al. 2009, 2011) and cancer research (Varga et al. 2005, 2006). Fenech et al. (2013) recently reviewed and summarized the most current developments in the automation of various MN assays by imaging cytometry and outlined a list of criteria that automated systems should be able to fulfill to ensure scoring accuracy. These criteria include, but are not limited to, the ability to detect the cytoplasm in addition to nuclei and MN, detection of MN in mononucleated cells and sufficient magnification to obtain a high degree of confidence for acceptance/rejection of MN. A number of other works have been presented on automating the CBMN assay for occupational and triage biological dosimetry. Both Schunck et al. (2004) and Varga et al. (2004) described an automated microscopy method for MN scoring using the MNScore software module integrated in the metaphase finder of the Metafer system (MetaSystems). This method automatically identifies binucleated cells (BNCs) through the occurrence of two adjacent nuclei stained with DAPI. The MN are then counted automatically by defining a circular region encompassing the two nuclei of the BNC. Willems et al. (2010) used this same system to develop a rapid population triage method via automated MN counting for the use following a large-scale radiation accident. They showed that automated MN scoring correlates very well with manual MN scoring and estimated that their method could allow for the processing of approximately 60 samples in a 12-h period.

A further advancement in automating the CBMN assay has been the Rapid Automated Biodosimetry Tool (RABiT), developed at Columbia University (Garty et al. 2010, 2011). This completely automated system can be used for both the CBMN and γH2AX assays for radiation biodosimetry. All processes following acquisition of fingerstick-derived blood samples are automated through the use of multi-well plates and robotics to estimate previous exposures or to identify exposures relative to a threshold dose. High-speed image analysis is performed online, and the system has the potential to analyze as many as 30,000 samples per day.

As early as 1984, there have been attempts to adapt the MN assay to traditional flow cytometry. One of the earliest publications was by Nüsse and Marx (1997) who developed an elegant flow cytometry method based on ethidium bromide fluorescence and forward and side scatter intensities to differentiate between debris, nuclei and MN. Although this method agreed well with microscopy, it was limited by artificially high readings from dead or dying cells as MN could not be distinguished from apoptotic bodies. More recently, this method has been built upon in several studies attempting to distinguish true MN from apoptotic and necrotic chromatin using ethidium monoazide that labels the chromatin of dead or dying cells in mouse lymphoblastoids (Avlasevich et al. 2006) and human TK6 cells (Bryce et al. 2007). While this modification improved the sensitivity of the assay, issues still existed in differentiating MN and free chromosomes from metaphase cells. While traditional flow cytometry increases the throughput of the CBMN assay as compared to microscopy-based methods, one major drawback is that cells require lysing prior to the analysis to release nuclei

and MN. This eliminates the ability to restrict analysis to BNCs and control for proliferation. Recent developments in flow technology have introduced imaging capabilities which take advantage of the traditional flow cytometry methodologies, while addressing some of the aforementioned limitations.

This paper introduces an automated method developed in our laboratory to perform the CBMN assay on the ImageStream^X imaging flow cytometry system for the purposes of radiation biodosimetry. The ImageStream^X combines the high-throughput advantages of traditional flow cytometry with the image analysis methods of standard microscopy-based methods. Modifications to existing standard protocols, as well as specific data collection and analysis parameters, are discussed.

Materials and methods

Blood collection and irradiation

For the CBMN assay, peripheral blood was collected from healthy anonymous donors in two 10-mL and one 4-mL lithium-heparinized vacutainer tubes (BD Biosciences, Mississauga, ON). Each sample was divided into 2.5-mL aliquots and irradiated at 0, 1, 2, 3, 4, 5, 6 and 7 Gy. Irradiation was performed using a cabinet X-ray machine (X-RAD 320, Precision X-Ray Inc., North Branford, CT, USA) at 250 kVp and 12.5 mA with a 2-mm Al filter. Each tube of blood was inserted on its side into the middle of 9 cm of water-equivalent build-up material resulting in a dose rate of 1.3 Gy/min calibrated using a UNIDOS PTW TW30010-10 ion chamber and T10002 electrometer (Freiburg, Germany) calibrated at the National Research Council, Ottawa, ON ($N_K = 48.3$ mGy/nC at 250 kV, assuming air kerma to be equal to dose).

CBMN assay

The CBMN assay was modified from the standard procedure of Fenech and Morley (1985) to allow for the analysis on the ImageStream^X (EMD-Millipore, Billerica, MA, USA) imaging flow cytometer. Whole blood samples were diluted 1:9 with RPMI 1640 culture medium containing 10 % fetal bovine serum, 2 mmol L-glutamine, 100 U/mL penicillin, 100 mg/mL streptomycin (Sigma-Aldrich, Oakville, ON) and 1 % phytohemagglutinin (PHA) (Life Technologies, Burlington, ON) to achieve 20 mL cultures in 25-cm^2 vented flasks. The cultures were incubated (37 °C, 5 % CO_2) for 24 h before the addition of cytochalasin B (4 μg/mL; Sigma-Aldrich) as recommended by the IAEA (2011). After an additional 48 h, cell suspensions were transferred to 50-mL polypropylene tubes and centrifuged at 200×*g* for 8 min. The supernatant was removed, and the cell pellets were resuspended in 30 mL of a 1× concentration of FACS lysing solution (BD Biosciences) then incubated at room temperature for 10 min. The samples were then washed twice at 1,300×*g* with 10 mL of phosphate-buffered saline (PBS) solution, and the pellet was resuspended in 100 μL of PBS. Lymphocyte cell concentrations were in the range of 1–2 × 10^7 cells/mL.

Data collection on Imagestream^X

The ImageStream^X flow cytometer is an imaging flow cytometry system capable of taking high-resolution photographs of individual cells at a rate of several hundred cells per second. All samples were stained with DRAQ5 (5 mM, eBioscience, San Diego, CA, USA) which has an affinity for double-stranded DNA. DRAQ5 was added to each 100 μL cell suspension to give a final concentration of 50 μM. All samples were run on the ImageStream^X at 40× magnification with the 658-nm laser set to 20 mW in channel 5 and the bright field (BF) LED in channel 1. Events with areas smaller than 100 pixels (25 μm^2) and larger than 2,000 pixels (500 μm^2) were excluded (note that 1 pixel = 0.25 μm^2). These parameters eliminated the collection of small debris and maximized BNC collection while maintaining a collection speed of approximately 100 events per second. The data were analyzed via a template developed in the IDEAS software package (EMD-Millipore).

Data analysis in IDEAS

An analysis template was designed in IDEAS which gated out undesirable events based on size, intensity, aspect ratio and DRAQ5 homogeneity and subsequently identified and automatically scored the MN frequency in BNCs in the remaining events. Once established, this template was used to analyze all data files. Detailed steps of the analysis are described below.

All events were first sorted using the *lobe count* feature applied to the DRAQ5 channel to differentiate cells with two distinct DRAQ5-stained nuclei from all other events in the data set (Fig. 1). Cytoplasmic material can be viewed in the BF channel; a histogram of the BF *aspect ratio* was created in order to distinguish between two mononucleated cells captured together in one image and a true BNC (Fig. 2). In IDEAS, the aspect ratio is defined as the length of the minor axis of the image divided by the length of the major axis of the image and is a measure of the roundness of the object. Therefore, single cells will be more round and have an aspect ratio close to 1, while two mononuclear cells captured together in the same image will be more elongated and have an aspect ratio closer to 0.5. All cells

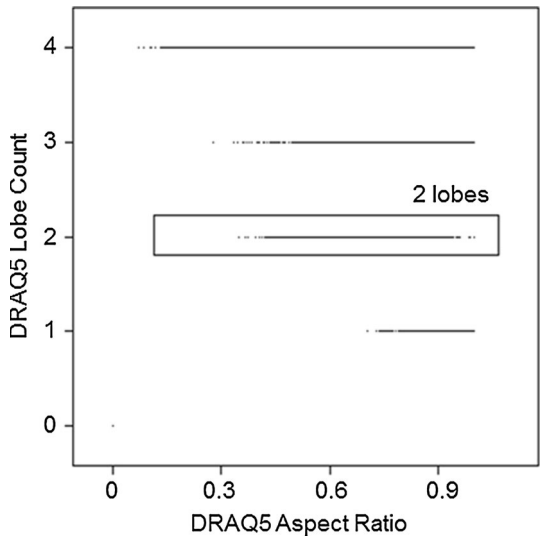

Fig. 1 Scatter plot of DRAQ5 *lobe count* versus *aspect ratio* showing the gate created to include all cells with two DRAQ5-stained nuclei and to exclude debris, single cells and cells with more than two nuclei

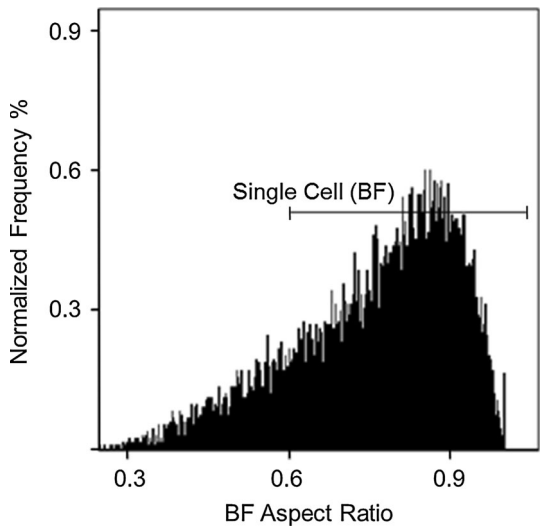

Fig. 2 Histogram of BF *aspect ratio* showing the gate created to distinguish single cells from two mononuclear cells captured together in the same image. *Aspect ratio* is defined as the length of the minor axis of the image divided by the length of the major axis of the image and describes how round an object is. Two mononuclear cells captured together in the same image would be found below the lower limit of the gate (i.e., below an aspect ratio of 0.6)

with an aspect ratio greater than 0.6 were determined to be true BNCs via optimization using a combination of the definition of aspect ratio and visual verification of the data. Initially, the lower limit was set to 0.5, but upon visual inspection, many events with two single cells captured together in the same image were passing through the filtering gate and being included as BNCs. When raising the

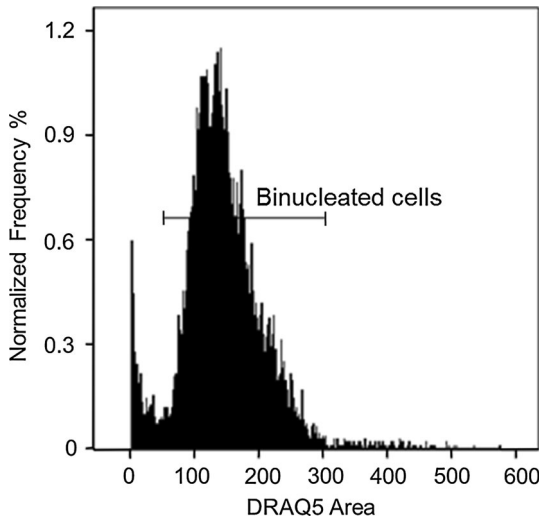

Fig. 3 Histogram of DRAQ5 area showing the gate encompassing cells between 50 and 300 μm^2 to exclude any small or large debris or cells

aspect ratio threshold to 0.7, these events were eliminated; however, many true BNCs were being filtered out due to their cytoplasm falling below the roundness threshold for an aspect ratio of 0.7. Thus, it was determined that an aspect ratio of 0.6 gave an optimal trade-off between gating out two mononuclear cells captured together in one image while allowing true BNCs to be carried forward in the analysis.

To remove any remaining debris, a histogram of DRAQ5 area was created, and any cells with an area of less than 50 μm^2 or greater than 300 μm^2 were rejected (Fig. 3). A scatter plot of cell *homogeneity* in the DRAQ5 channel versus cell *width* in the DRAQ5 channel was generated (Fig. 4). *Homogeneity* is a texture feature based on the local intensity in the DRAQ5 images. BNCs with two well-defined nuclei have a more uniform intensity profile and a higher homogeneity as compared to debris and other cells where the nuclei are not well separated from each other inside the cytoplasm. Thus, cells with a mean homogeneity lower than 10 were deemed to be less than ideal BNCs and were excluded. The *width* feature creates an elongated rectangle around the two nuclei in the DRAQ5 channel and calculates the length of the shorter side. Nuclei with widths less than 12 μm or greater than 18 μm were determined not to be BNCs and were excluded. Finally, a plot of DRAQ5 *compactness* versus DRAQ5 aspect ratio intensity was generated (Fig. 5). *Compactness* of DRAQ5 measures the degree of how well the object is packed together and allows for differentiation from well-rounded objects, such as cells with a single nucleus, to more irregular objects, such as binucleated cells. Most BNCs were found to have a DRAQ5 compactness between

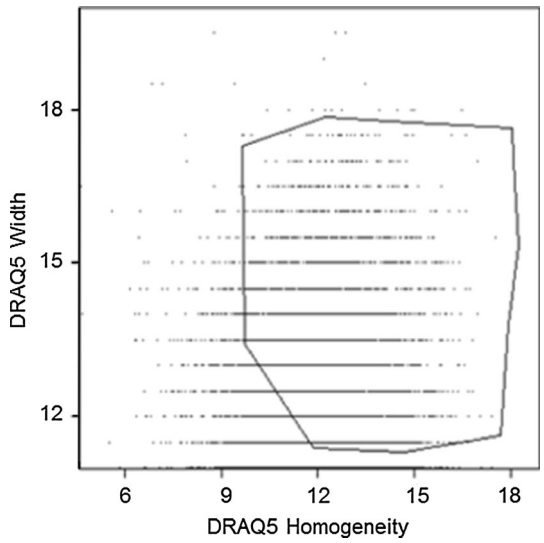

Fig. 4 Scatter plot of DRAQ5 *width* versus *homogeneity* illustrating the gate to include cells with more uniform distribution of DRAQ5 stain (homogeneity greater than 10) and to reject cells that were too small or too large (width less than 12 μm or greater than 18 μm, respectively)

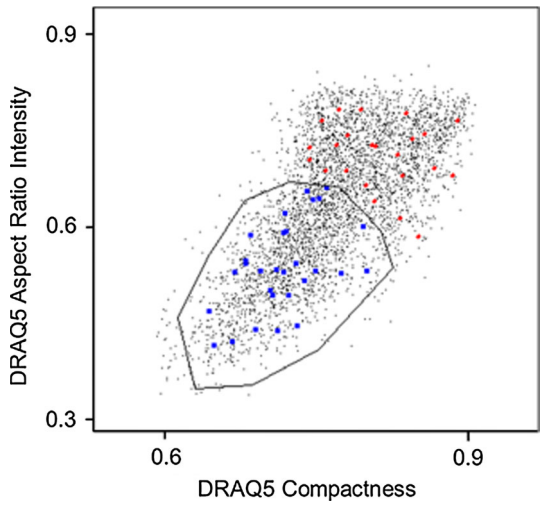

Fig. 5 Scatter plot of DRAQ5 *aspect ratio* intensity versus *compactness* with the gate created to encompass the acceptable BNC population (solid blue squares inside gate). Cells highlighted by solid red diamonds are not BNCs and fall outside the gate (color figure online)

0.6 and 0.8, so all events outside of this range were rejected. The DRAQ5 aspect ratio intensity is typically employed to distinguish single nuclei from double nuclei. The majority of BNCs were found to have an aspect ratio intensity between 0.4 and 0.7, and events outside of this range were excluded. Figure 5 also illustrates how a selected population of BNCs (solid blue squares) falls well within the gate and a selected population of non-BNCs (solid red triangles) falls outside of the gate. The gating strategy presented here effectively selects for BNCs while eliminating small and large debris, single cells and other non-desirable objects within each data set. Using the gated data, a masking system developed in IDEAS was used to identify MN in each image.

The IDEAS software contains a large selection of criteria for image analysis, called features, which generate quantitative and positional information about an image. Features are applied to locations of an image through the use of masks, which identify pixels within the region of interest of the image. To perform automated MN identification and counting, a series of masks were created in IDEAS. First, a DRAQ5 intensity threshold was applied to remove any debris that remained in the population following the gating strategy described above. Next, spot masking was used to identify both DRAQ5-stained MN and BNCs. The spot mask makes use of the spot-to-cell background ratio, which is the spot pixel value divided by the background, as well as the radius value of the spot. A DRAQ5 MN mask was created to identify spots in images that had a spot-to-cell background value of at least 1.5 and a radius of at least 8 pixels. Using these parameters, an area range was then defined to identify spots having an area between 10 and 100 pixels, to be consistent with the criteria for MN scoring (Fenech 2007). In a similar fashion, a BNC spot mask was created to identify images that contained two distinguishable DRAQ5-stained nuclei within a single cell. Here, the spot-to-cell background ratio was set to at least 2.5, and the radius was set to a minimum of 18 pixels to mask both nuclei while excluding any MN from the mask. A threshold area was set to 300 pixels, sufficient to mask all nuclei. Figure 6a shows a BNC with one MN, Fig. 6b shows the MN mask, and Fig. 6c shows the BNC mask. Finally, to count the MN in each data set, a *spot count* feature was applied, which counted all masked MN. A histogram of MN frequency was then plotted, with a gate on each bin from 0 to 4 MN per BNC. The gate on the 4 MN bin is inclusive of 4 or more MN per BNC (Fig. 7).

Results

The ImageStream^X allows the opportunity to visualize particles on several channels as they pass through the cytometer. The BF channel allows for both imaging of the cytoplasm and composite image generation in which the DRAQ5-stained nuclei and MN can be overlayed to clearly distinguish between true BNCs with MN (first to third rows of Fig. 8) and two individual mononuclear cells captured in the same image (fifth row of Fig. 8). It is straightforward to identify mononuclear cells and associated MN (fourth row of Fig. 8) as well as multi-nucleated cells (sixth row of

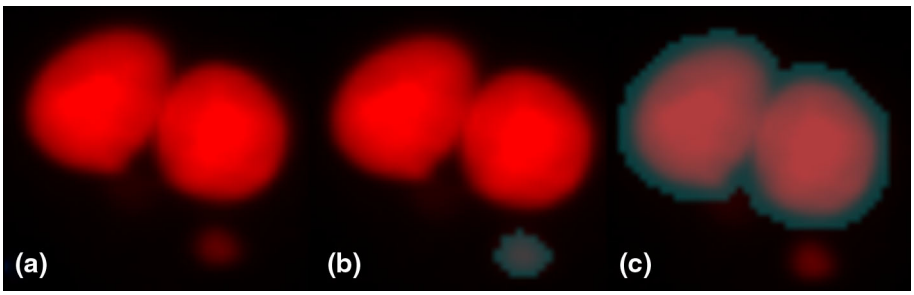

Fig. 6 **a** A DRAQ5-stained BNC with a single MN. **b** The MN mask highlighting the MN. **c** The BNC mask encompassing the two nuclei

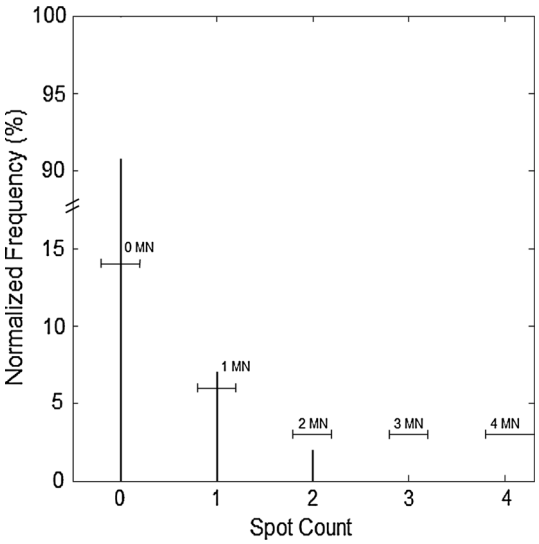

Fig. 7 Histogram of the *spot count* feature created using the BNC and MN masks for a sample irradiated with 4 Gy. The gates shown are used to count the number of BNCs (0 MN) and the number of MN in each bin. The gate on the 4 MN bin counts all cells with 4 or more MN. The normalized frequency represents the percentage of each type of cell from the total number of cells in the population

Fig. 8) by simply creating additional gates using the lobe count feature.

To improve delineation of the cytoplasm, the use of cytoplasm stains and cell surface markers was investigated. While all stains employed were easily visualized by the ImageStream^X, uniformity of the stain was not as good as expected and offered little enhancement over the gating strategies developed using the BF images. Furthermore, the staining steps added additional time and cost to the sample preparation method for no significant gain, which is undesirable for the applications of this method to rapid triage biodosimetry.

Four independent experiments were conducted employing the methods described above. Figure 9 shows the data from the individual experiments as well as the dose response curve that is a weighted average of the four data sets generated for doses between 0 Gy and 4 Gy. The ordinate is presented as the rate of MN per BNC, and the data follow a linear-quadratic function ($R^2 = 0.994$); however, examination of the equation of the fit reveals that the linear term contributes to the fit more than the quadratic term. Given the early stages of this work, the increasing frequency of MN per BNC with dose is encouraging and indicates that this method is sensitive enough to distinguish between a 0 Gy and 2 Gy irradiated sample, which would be sufficient for rapid casualty triage. Figure 10 shows the results from 0 Gy to 7 Gy, which is also a weighted average of the four data sets. It can be seen that the MN frequency increased up to 4 Gy and then starts to decrease at higher doses.

Discussion

An automated, imaging flow cytometry method for performing the CBMN assay for the purposes of radiation biodosimetry has been presented. In situations where large numbers of casualties may need to be assessed for possible radiation exposure, a method that is quick and robust is desirable.

In a recent publication, Fenech et al. (2013) provided a comprehensive review of several automated MN assays that use imaging cytometry systems. As mentioned previously, they also developed a list of criteria that all imaging systems should be able to fulfill to ensure accurate, reliable and reproducible results. While the method presented here does not use slide-based scoring, it does satisfy a number of the outlined criteria, as explained below. Imaging of the cytoplasm is as important as imaging the nuclei and MN, such that mono-, bi- and multi-nucleated cells can be identified and quantified. It has been demonstrated that this can be accomplished with the ImageStream^X. Another consideration that Fenech et al. (2013) pointed out is that imaging cytometry systems should have a high detection efficiency for MN in both mononucleated cells and BNCs. The frequency of MN per BNC measured by the ImageStream^X is currently one full order of magnitude lower than traditional microscopy-based methods of CBMN for radiation biodosimetry (McNamee et al. 2009; Vral et al. 2011). Studies by Varga et al. (2004) and Schunck et al. (2004), in which the Metafer system was used to automate

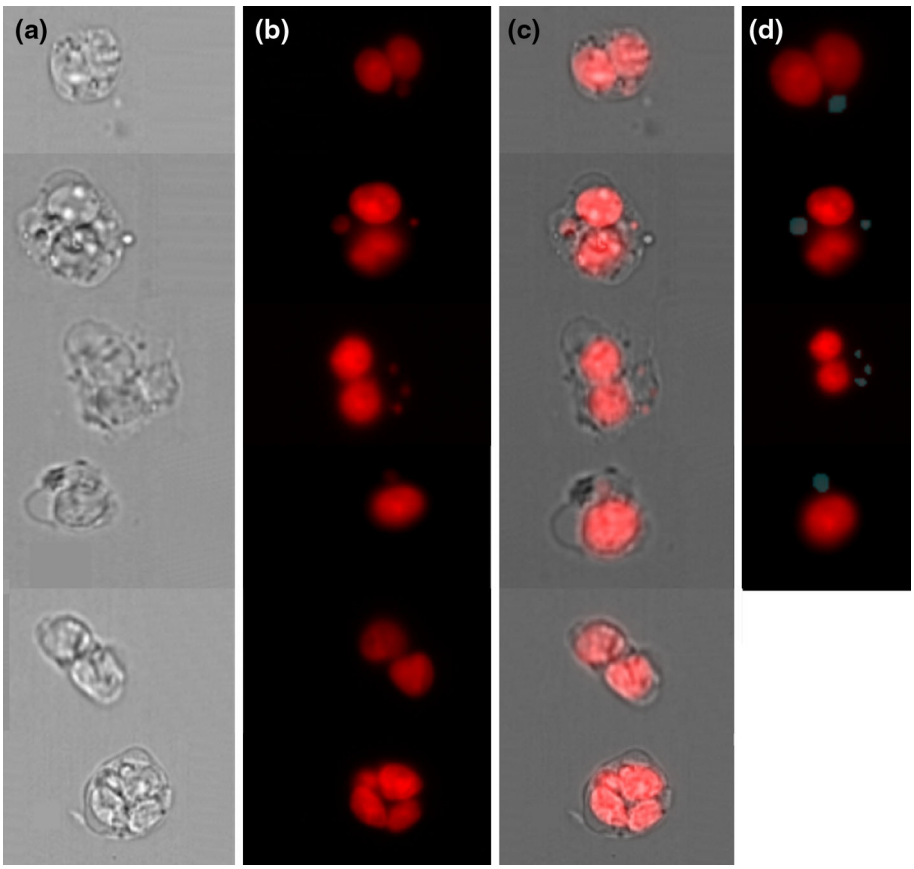

Fig. 8 Various images captured by the ImageStream^X. **a** BF images clearly depicting the cytoplasm boundaries around the nuclei. **b** DRAQ5-stained nuclei and MN. **c** Composite BF/DRAQ5 images created to illustrate the use of the BF image to delineate the cytoplasm surrounding the nuclei. **d** *First row* a BNC with one masked MN, *second row* a BNC with two masked MN, *third row* a BNC with three masked MN, *fourth row* a mononuclear cell with one masked MN, *fifth row* two mononuclear cells captured in the same image, *sixth row* a tetranucleated cell

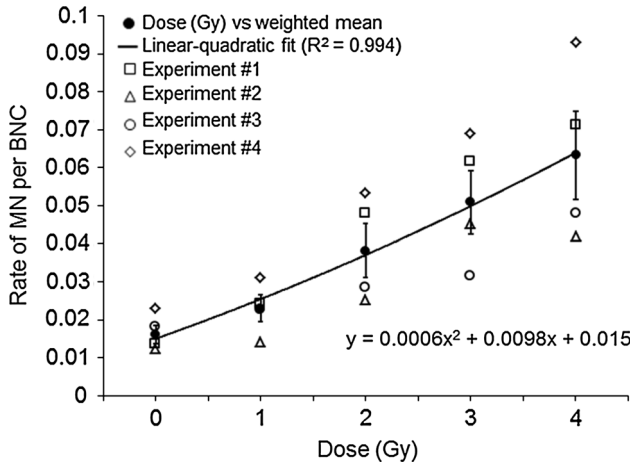

Fig. 9 Data from four experiments as well as the dose response curve from 0 to 4 Gy, which represents the weighted mean number of MN/BNC identified for each dose. Error bars represent the standard error of the mean, and the curve is fit with a linear-quadratic function ($R^2 = 0.994$)

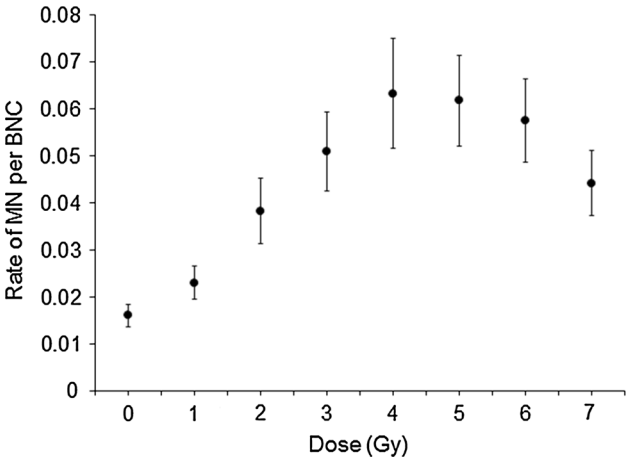

Fig. 10 Data from four experiments from 0 to 7 Gy. Shaded circles represent the weighted average number of MN/BNC identified for a given dose, and the error bars represent the standard error of the mean

the slide-scoring method for CBMN, both reported lower rates of MN as compared to the traditional manual scoring method. According to the authors, the stricter scoring parameters applied in image analysis can cause some MN that would normally be counted manually, to be missed. For example, MN in contact with the nuclei would normally be counted manually, but are excluded by virtue of the automated scoring parameters. In this work, the lower MN frequency may also be due to some of the true BNCs being removed from the final population as a result of the gating strategy. It may also be as a result of the cells being

in solution as opposed to on slides. In this three-dimensional system, some MN may be hidden behind a nucleus such that they cannot be visualized or MN may be at a different depth of field than the nuclei and are not intense enough to be clearly identified and masked. Additional data were collected using the extended depth of field option on the ImageStream^X, but no improvement in MN frequency or image quality was observed. Therefore, the lower MN frequency may simply be a general phenomenon of automated analysis methods. Beaton et al. (2013) recently reported on this same trend while performing the DCA on the ImageStream^X. This is likely not a major drawback for the purposes of triage biodosimetry as the low MN frequency would be accounted for in the dose response curve. All samples would be analyzed using the same IDEAS template employed to generate the curve and the results compared to the curve itself; thus, the low MN frequency likely becomes irrelevant. Further, in a mass casualty event, the distinction between low ($\sim$0 Gy) and high doses (>2 Gy) must be made quickly (Sullivan et al. 2013). The dose response curve shown in Fig. 9 indicates that the automated method developed in this work is capable of rapidly making the distinction between 0 Gy and 2 Gy. Further, it can be argued that in a situation where a casualty has received a total body dose of greater than 4 Gy, such as a radiation accident, the deterministic effects would trigger medical intervention long before the 72-h incubation period required for the CBMN assay is complete and rapid dose determination becomes less important than accuracy (Hall and Giaccia 2006). Conversely, when optimizing the method to determine its sensitivity, the low MN frequency will likely play a significant role. It is possible that the MN frequency can be increased by further refining and optimizing the analysis strategy to detect any smaller MN that may be gated out or missed by the masking.

In order to obtain maximum confidence to accept or reject objects as MN, a sufficiently high magnification must be employed in all imaging cytometry methods (Fenech et al. 2013). The ImageStream^X has three objectives (20×, 40× and 60×), all of which were investigated for their ability to image BNCs and MN with sufficient resolution. The 40× objective proved to give the best combination of acquisition speed and image resolution. At higher magnification, a reduction in collection speed was observed and therefore, to obtain sufficient image quality while maintaining high throughput, all data were collected using settings optimized for the 40× objective.

Apart from the measurement of MN, the CBMN assay has been adapted to quantify other important biomarkers such as nucleoplasmic bridges, nuclear buds and necrotic or apoptotic cells (Fenech et al. 2013). While the measurement of these falls outside of the scope of this paper, the breadth of applications within the IDEAS software package may indeed make it possible in future to quantify these structures.

At high doses of radiation, it can be seen that the frequency of MN per BNC falls off, specifically after 5 Gy (Fig. 10). The number of BNCs acquired and scored also decreased beyond 5 Gy. This is consistent with results of dose response curves recently generated by Lyulko et al. (2014) and Müller and Rode (2002) in which similar trends were observed up to 10 Gy and 15 Gy, respectively. The reduction in BNC and MN frequency at higher doses can likely be explained by the effect of radiation on cell proliferation and the inability of the cells to pass through karyokinesis (Müller and Rode 2002). Müller and Rode (2002) have suggested that higher doses can be estimated through scoring the fraction of mononuclear cells as well as the ratio of trinucleated to tetranucleated cells following radiation exposure. It has been shown in this work that these structures can be detected and imaged using the ImageStream^X. Therefore, accurately estimating doses higher than 5 Gy is likely possible though the development of an IDEAS template that can evaluate all of these criteria simultaneously, which would be significantly faster than manual scoring.

In addition to satisfying the aforementioned criteria, performing the CBMN assay on the ImageStream^X has other advantages. It combines the speed of sample preparation with a data analysis method that is free of user intervention or individual bias. Willems et al. (2010) recently estimated that their automated MN scoring procedure could allow 2 technicians to process approximately 60 samples in a 12-h shift. We estimate that the imaging flow cytometry CBMN method developed here can allow for the complete analysis of at least the same amount of samples, perhaps even more, in a 12-h period due to the fact that the flow CBMN method does not require slide preparation time. With the condensed method employed in this work, approximately 2 h was needed to completely process the 8 samples used to generate Fig. 10, from the end of incubation to a stage where they were ready to be run on the ImageStream^X. Once ready for analysis on the ImageStream^X, each sample can take between 10 and 20 min to acquire and another 5–10 min to analyze with the IDEAS analysis template. The data collection and analysis time for all doses presented here (0–7 Gy) was approximately 2 h. Thus, a total of about 4 h was required to generate Fig. 10 by a single person working alone in the laboratory from end of incubation to final results.

An average of 1,800 BNCs was counted in the analysis template for each dose point, but the number of cells detected is much higher. The gating strategy removes many unsuitable cells (e.g., mononuclear cells), and further improvements to the analysis template should increase the efficiency of separating more BNCs from debris and other non-desirable events. Still, 1,800 BNCs is nearly double

the number of BNCs that are scored per sample by conventional microscope-based CBMN. Future refinement of the data collection parameters on the ImageStream^X, as well as the analysis template, may make it possible to automatically identify, count and analyze 1,000 BNCs and associated MN in 15 min per sample. Furthermore, the IDEAS software possesses a batch processing mode that has the capability to process several data files simultaneously and to save the statistical data as a report. This batch processing mode in combination with the use of a 96-well plate could allow even further improvements in throughput. Still, as with all methods to perform the CBMN assay, the 72-h sample incubation time remains the major limiting factor on the overall speed of the assay. Hence, a reduction in the time from incubation to results is of utmost importance in a mass casualty event, and the imaging flow CBMN method presented in this paper could conceivably generate a dose estimation for a single individual in as little as 2 h following the incubation time.

The results presented in this paper indicate that imaging flow cytometry can be used to automate the CBMN assay for the purposes of rapid triage biodosimetry. This work compliments other recent publications in which imaging flow cytometry has been used to automate the DCA (Beaton et al. 2013) and other slide-based techniques that have been developed to automate the CBMN and γH2AX assays (Garty et al. 2010, 2011; Lyulko et al. 2014) for the purposes of radiation biodosimetry. Further work is required to optimize the masking and analysis template to possibly increase the MN detection frequency. Additional experiments will be performed in an attempt to accurately estimate high radiation doses (>5 Gy) by developing a template that simultaneously analyzes the data based on several criteria mentioned previously. Finally, determination of the sensitivity of the method at very low doses and validation via blinded samples will be performed.

Acknowledgments The authors wish to thank Richard DeMarco (Amnis Corp., EMD-Millipore) for his help with the gating and masking strategies in the IDEAS software.

References

Avlasevich SL, Bryce SM, Cairns SE, Dertinger SD (2006) In vitro micronucleus scoring by flow cytometry: differential staining of micronuclei versus apoptotic and necrotic chromatin enhances assay reliability. Environ Mol Mutagen 47(1):56–66. doi:10.1002/em.20170

Beaton LA, Ferrarotto C, Kutzner BC, McNamee JP, Bellier PV, Wilkins RC (2013) Analysis of chromosome damage for biodosimetry using imaging flow cytometry. Mutat Res Genet Toxicol Environ Mutagen. doi:10.1016/j.mrgentox.2013.04.002

Bryce SM, Bemis JC, Avlasevich SL, Dertinger SD (2007) In vitro micronucleus assay scored by flow cytometry provides a comprehensive evaluation of cytogenetic damage and cytotoxicity. Mutat Res Genet Toxicol Environ Mutagen 630(1–2):78–91. doi:10.1016/jmrgentox.2007.02.002

Castelain P, Vanhummelen P, Deleener A, Kirschvolders M (1993) Automated detection of cytochalasin-B blocked binucleated lymphocytes for scoring micronuclei. Mutagenesis 8(4):285–293. doi:10.1093/mutage/8.4.285

EA IA (2011) Cytogenetic dosimetry: applications in preparedness for and response to radiation emergencies. IAEA, Vienna

Fenech M (2007) Cytokinesis-block micronucleus cytome assay. Nat Protoc 2(5):1084–1104. doi:10.1038/nprot.2007.77

Fenech M, Morley AA (1985) Measurement of micronuclei in lymphocytes. Mutat Res 147(1–2):29–36. doi:10.1016/0165-1161(85)90015-9

Fenech M, Kirsch-Volders M, Rossnerovac A, Sram R, Romm H, Bolognesi C, Ramakumar A, Soussaline F, Schunck C, Elhajouji A, Anwar W, Bonassi S (2013) HUMN project initiative and review of validation, quality control and prospects for further development of automated micronucleus assays using image cytometry systems. Int J Hyg Environ Health 216:541–552

Garty G, Chen YH, Salerno A, Turner H, Zhang J, Lyulko O, Bertucci A, Xu YP, Wang HL, Simaan N, Randers-Pehrson G, Yao YL, Amundson SA, Brenner DJ (2010) The RABIT: a rapid automated biodosimetry tool for radiological triage. Health Phys 98(2):209–217. doi:10.1097/HP.0b013e3181ab3cb6

Garty G, Chen YH, Turner HC, Zhang J, Lyulko OV, Bertucci A, Xu YP, Wang HL, Simaan N, Randers-Pehrson G, Yao YL, Brenner DJ (2011) The RABiT: a rapid automated biodosimetry tool for radiological triage. II. TECHNOLOGICAL developments. Int J Radiat Biol 87(8):776–790. doi:10.3109/09553002.2011.573612

Hall EJ, Giaccia AJ (2006) Radiobiology for the radiologist, 6th edn. Lippincott Williams & Wilkins, Philadelphia

Lloyd DC, Edwards AA, Moquet JE, Guerrero-Carbajal YC (2000) The role of cytogenetics in early triage of radiation casualties. Appl Radiat Isot 52(5):1107–1112. doi:10.1016/s0969-8043(00)00054-3

Lyulko OV, Garty G, Randers-Pehrson G, Turner HC, Szolca B, Brenner DJ (2014) Fast image analysis for the micronucleus assay in a fully automated high-throughput biodosimetry system. Radiat Res [Epub ahead of print]

McNamee JP, Flegal FN, Greene HB, Marro L, Wilkins RC (2009) Validation of the cytokinesis-block micronucleus (CBMN) assay for use as a triage biological dosimetry tool. Radiat Prot Dosim 135(4):232–242. doi:10.1093/rpd/ncp119

Müller WU, Rode A (2002) The micronucleus assay in human lymphocytes after high radiation doses (5–15 Gy). Mutat Res Fundam Mol Mech Mutagen 502(1–2):47–51. doi:10.1016/s0027-5107(02)00022-2

Nüsse M, Marx K (1997) Flow cytometric analysis of micronuclei in cell cultures and human lymphocytes: advantages and disadvantages. Mutat Res Genet Toxicol Environ Mutagen 392(1–2):109–115. doi:10.1016/s0165-1218(97)00049-9

Rossnerova A, Spatova M, Rossner P, Solansky I, Sram RJ (2009) The impact of air pollution on the levels of micronuclei measured by automated image analysis. Mutat Res Fundam Mol Mech Mutagen 669(1–2):42–47. doi:10.1016/j.mrfmmm.2009.04.008

Rossnerova A, Spatova M, Pastorkova A, Tabashidze N, Veleminsky M, Balascak I, Solansky I, Sram RJ (2011) Micronuclei levels in mothers and their newborns from regions with different types of air pollution. Mutat Res Fundam Mol Mech Mutagen 715(1–2):72–78. doi:10.1016/j.mrfmmm.2011.07.011

Schunck C, Johannes T, Varga D, Lorch T, Plesch A (2004) New developments in automated cytogenetic imaging: unattended scoring of dicentric chromosomes, micronuclei, single cell gel electrophoresis, and fluorescence signals. Cytogenet Genome Res 104(1–4):383–389. doi:10.1159/000077520

Sullivan J, Prasanna P, Grace M, Lynne Wathen, Wallace R, Koerner J, Coleman C (2013) Assessment of biodosimetry methods for a mass-casualty radiological incident: medical response and management considerations. Health Phys 105(6):540–554. doi:10.1097/HP.0b013e31829cf221

Varga D, Johannes T, Jainta S, Schuster S, Schwarz-Boeger U, Kiechle M, Garcia BP, Vogel W (2004) An automated scoring procedure for the micronucleus test by image analysis. Mutagenesis 19(5):391–397. doi:10.1093/mutage/geh047

Varga D, Michel I, Patino-Garcia B, Paiss T, Vogel W, Maier C (2005) Radiosensitivity detected by the micronucleus test is not generally increased in sporadic prostate cancer patients. Cytogenet Genome Res 111(1):41–45

Varga D, Hoegel J, Maier C, Jainta S, Hoehne M, Patino-Garcia B, Michel I, Schwarz-Boeger U, Kiechle M, Kreienberg R, Vogel W (2006) On the difference of micronucleus frequencies in peripheral blood lymphocytes between breast cancer patients and controls. Mutagenesis 21(5):313–320

Vaurijoux A, Gruel G, Pouzoulet F, Gregoire E, Martin C, Roch-Lefevre S, Voisin P, Roy L (2009) Strategy for population triage based on dicentric analysis. Radiat Res 171(5):541–548. doi:10.1667/rr1664.1

Vaurijoux A, Gregoire E, Roch-Lefevre S, Voisin P, Martin C, Roy L, Gruel G (2012) Detection of partial-body exposure to ionizing radiation by the automatic detection of dicentrics. Radiat Res 178(4):357–364. doi:10.1667/rr2728.1

Verhaegen F, Vral A, Seuntjens J, Schipper NW, Deridder L, Thierens H (1994) Scoring of radiation-induced micronuclei in cytokinesis-blocked human-lymphocytes by automated image-analysis. Cytometry 17(2):119–127. doi:10.1002/cyto.990170203

Vral A, Fenech M, Thierens H (2011) The micronucleus assay as a biological dosimeter of in vivo ionising radiation exposure. Mutagenesis 26(1):11–17. doi:10.1093/mutage/geq078

Willems P, August L, Slabbert J, Romm H, Oestreicher U, Thierens H, Vral A (2010) Automated micronucleus (MN) scoring for population triage in case of large scale radiation events. Int J Radiat Biol 86(1):2–11. doi:10.3109/09553000903264481